# *Distinct Roles of RZZ and Bub1-KNL1 in Mitotic Checkpoint Signaling and Kinetochore Expansion*

HHS Public Access

Author manuscript

*Curr Biol*. Author manuscript; available in PMC 2019 November 05.

Published in final edited form as:

*Curr Biol*. 2018 November 05; 28(21): 3422–3429.e5. doi:10.1016/j.cub.2018.10.006.

# Distinct roles of RZZ and Bub1-KNL1 in mitotic checkpoint signaling and kinetochore expansion

**Jose-Antonio Rodriguez-Rodriguez**[1], **Clare Lewis**[1], **Kara L. McKinley**[2,3], **Vitali Sikirzhytski**[4,5], **Jennifer Corona**[1], **John Maciejowski**[1], **Alexey Khodjakov**[4,5], **Iain M. Cheeseman**[2,3], and **Prasad V. Jallepalli**[1,*]

[1]Molecular Biology Program, Sloan Kettering Institute, Memorial Sloan Kettering Cancer Center, New York, NY, 10065, USA

[2]Whitehead Institute for Biomedical Research, Nine Cambridge Center, Cambridge, MA 02142, USA

[3]Department of Biology, Massachusetts Institute of Technology, Cambridge, MA 02142, USA

[4]Wadsworth Center, New York State Department of Health, Albany, NY 12201

[5]Rensselaer Polytechnic Institute, Troy, NY 12180

## Summary

The Mad1-Mad2 heterodimer is the catalytic hub of the spindle assembly checkpoint (SAC), which controls M phase progression through a multi-subunit anaphase inhibitor, the mitotic checkpoint complex (MCC) [1, 2]. During interphase, Mad1-Mad2 generates MCC at nuclear pores [3]. After nuclear envelope breakdown (NEBD), kinetochore-associated Mad1-Mad2 catalyzes MCC assembly until all chromosomes achieve bipolar attachment [1, 2]. Mad1-Mad2 and other factors are also incorporated into the fibrous corona, a phospho-dependent expansion of the outer kinetochore that precedes microtubule attachment [4–6]. The factor(s) involved in targeting Mad1-Mad2 to kinetochores in higher eukaryotes remain controversial [7–12], and the specific phosphorylation event(s) that trigger corona formation remain elusive [5, 13]. We used genome editing to eliminate Bub1, KNL1, and the Rod-Zw10-Zwilch (RZZ) complex in human cells. We show that RZZ's sole role in SAC activation is to tether Mad1-Mad2 to kinetochores. Separately, Mps1 kinase triggers fibrous corona formation by phosphorylating two N-terminal sites on Rod. In contrast Bub1 and KNL1 activate kinetochore-bound Mad1-Mad2 to produce a "wait anaphase" signal, but are not required for corona formation. We also show that clonal lines isolated after *BUB1* disruption recover Bub1 expression and SAC function through nonsense-

*corresponding author and lead contact: jallepap@mskcc.org.

Author Contributions

J.-A.R.-R., C.L., K.L.M., J.C., J.M., and P.V.J. performed molecular biology, cell imaging, and biochemical studies and analyzed data. V.S. performed electron microscopy and analyzed data. A.K., I.M.C., and P.V.J. planned and supervised research, analyzed data, and secured funding. J.-A.R.-R. and P.V.J. wrote the paper with input from all authors.



Declaration of Interests

The authors declare no competing interests.

associated alternative splicing (NAS). Our study reveals a fundamental division of labor in the mammalian SAC and highlights a transcriptional response to nonsense mutations that can reduce or eliminate penetrance in genome editing experiments.

## eTOC

Rodriguez-Rodriguez et al. identify distinct roles for Bub1, KNL1, and RZZ in SAC signaling and fibrous corona formation. They also show that BUB1-disrupted clones re-express Bub1 and regain SAC function via nonsense-associated alternative splicing, a often-overlooked transcriptional response that can limit penetrance in genome editing experiments

## Results

### The RZZ complex is required to maintain SAC arrest but not to initiate it

To analyze RZZ's roles in fibrous corona assembly and SAC signaling, we used AAV and CRISPR/Cas9 to modify both alleles of *KNTC1* (Rod) in HCT116 cells, a diploid human colorectal cell line (Figure S1A-C). *KNTC1*$^{HF/-}$ (hypomorph-flox) cells expressed Rod at ~20% of the wildtype level (Figure S1D) and exited mitosis prematurely when microtubule polymerization (nocodazole, 99±6 min s.e.m.) or spindle bipolarity (S-trityl-L-cysteine (STLC), 193±9 min) were inhibited. In contrast wildtype cells never exited mitosis during the 16-hour timelapse (Figure 1A). We obtained viable *KNTC1*$^{-/-}$ clones after expressing Cre recombinase, which were as SAC-defective as *KNTC1*$^{HF/-}$ cells (Figure 1A and Figure S1E). Early escape from spindle poison-induced mitotic arrest was also observed in *KNTC1*$^{-/-}$ human retinal pigment epithelial (RPE) cells and *KNTC1*, *ZW10*, and *ZWILCH* KO HeLa cells (Figure 1B-C and Figure S1F-I). On the other hand, untreated RZZ-null cells had longer and more heterogenous mitotic timing, suggesting frequent but transient SAC activation (Figure 1D). Consistently, inhibiting the SAC kinase Mps1 caused *KNTC1*$^{-/-}$ cells to exit mitosis with wildtype kinetics (Figure 1D). These observations suggest that RZZ maintains (but does not initiate) SAC signaling at unattached or improperly attached kinetochores in multiple human cell types.

### RZZ mediates a temporal switch in how Mad1-Mad2 is targeted to kinetochores

To understand RZZ's impact on mitotic chromosome and SAC signaling dynamics, we expressed and imaged H2B-mCherry and FLAP (FLAG-GFP-TEV-S peptide)-Mad1 using spinning disk confocal microscopy. Mad1 first localized at kinetochores at nuclear envelope breakdown (NEBD), then dissociated as chromosomes congressed at the metaphase plate (Figure 1E and Video S1; n=10 cells). Congression was less efficient in *KNTC1*$^{-/-}$ cells, consistent with the lack of Spindly and dynein at kinetochores ([14] and Figure S1F-I), but Mad1 was still targeted to misaligned chromosomes as effectively as in wildtype cells (Figure 1F-G and Video S2; n=14 cells). We conclude that early mitotic cells can recruit Mad1-Mad2 to kinetochores and inhibit anaphase onset in the absence of the RZZ complex.

Next we analyzed Mad1 dynamics in cells undergoing nocodazole-induced SAC arrest. Mad1 initially localized to kinetochores at NEBD in both wildtype and *KNTC1*$^{-/-}$ cells, but this localization was not persistently maintained in the absence of RZZ (Figure 1H). To

confirm this result for endogenous Mad1, wildtype and *KNTC1*$^{-/-}$ RPE cells were treated with nocodazole and MG132 (to block mitotic exit) for 30 min or 4 hours, then fixed and analyzed by immunofluorescence microscopy (IFM). In wildtype cells Mad1 formed large crescents that were stable over time, whereas it formed compact foci in *KNTC1*$^{-/-}$ cells that were eventually lost from kinetochores (Figure 1I-J). Suppressing early mitotic Mad1-Mad2 recruitment by treatment with Aurora B inhibitors [15, 16] eliminated the residual SAC response in *KNTC1*$^{-/-}$ cells ($T_{mitosis}$=39±10 min; Figure 1K). These results reveal a temporal switch from RZZ-independent to RZZ-dependent recruitment of Mad1-Mad2 during chronic SAC signaling.

## Mps1 promotes kinetochore expansion by phosphorylating the N-terminus of Rod

Mad1-Mad2 and RZZ localize to the fibrous corona, a phosphodependent expansion of the outermost kinetochore layer that persists until end-on microtubule attachments are formed [5, 6, 17]. Kinetochore expansion is thought to accelerate mitotic ‘search and capture’ by promoting lateral microtubule attachment [4] and to enhance SAC signaling [5]. RZZ is closely related to endomembrane coatomers that form oligomeric lattices [18, 19] and is likely a “building block” of the corona itself [13, 14, 20, 21]. Consistent with these proposals, two other corona-associated proteins (CENP-E [22] and CENP-F [23]) did not form crescents in *KNTC1*$^{-/-}$ cells (Figure 2A-B and S2A). To ensure that these results reflected loss of kinetochore expansion and not protein mislocalization, we performed correlative light-electron microscopy in cells expressing CENP-A-GFP as a centromere marker. Serial sectioning revealed circumferential expansion of trilaminar plates and fibrous material in wildtype cells (n=14 kinetochores), whereas the kinetochores of *KNTC1*$^{-/-}$ cells appeared as compact discs (n=15; Figure S2B and [13]). We conclude that the RZZ complex is required for fibrous corona formation.

In parallel we looked for mitotic kinases that might activate RZZ for kinetochore expansion. We found that CENP-E kinetochore crescents become compact after treating cells with an Mps1 inhibitor, but not after treatment with an Aurora B inhibitor (Figure 2C-D and [13]). Through global phosphoproteomic screening, we identified two Mps1-modified sites at the N-terminus of Rod (T13 and S15), upstream of its β-propeller domain [24]. To test the function of these sites, wildtype (WT) and nonphosphorylatable (2A) versions of Rod were expressed in T-Rex FLP-in HeLa cells as LAP (EGFP-TEV-S-peptide) fusions (Figure S2C). Both LAP-Rod$^{WT}$ and LAP-Rod$^{2A}$ were incorporated into the full RZZ complex based on co-immunoprecipitation assays (Figure S2D). We then disrupted the *KNTC1* locus in these cells using CRISPR/Cas9 and isolated transgene-complemented clones. Although LAP-Rod$^{WT}$ and LAP-Rod$^{2A}$ both localized to unattached kinetochores in the absence of endogenous Rod, only LAP-Rod$^{WT}$ formed crescents (Figure 2E-F). Thus far the only post-translational modification known to be required for crescent formation is C-terminal farnesylation of Spindly, which enables its kinetochore recruitment via interaction with Rod’s β-propeller domain [14, 20, 25, 26]. However Rod$^{2A}$ recruited Spindly and other corona-associated proteins in proportion to its own reduced abundance (Figure 2F). Despite having lower levels of Mad1-Mad2, the compact kinetochores in Rod$^{2A}$ cells sustained mitotic arrest in nocodazole as effectively as those in Rod$^{WT}$ cells (Figure 2G). We conclude

that Rod's N-terminal phosphorylation is required for fibrous corona formation but not SAC signaling.

## Mad1-Mad2 requires a non-receptor activity of Bub1 to inhibit anaphase

Bub1 is required for kinetochore expansion in *Xenopus* egg extracts [5] but its role in fibrous corona formation in human cells has not been examined. Bub1's role in the SAC also remains controversial, with inconsistent results across studies [7–12]. To test Bub1's contribution to these aspects of kinetochore structure and function, we deleted *BUB1* in RPE cells via doxycycline-inducible CRISPR/Cas9 [27]. *BUB1*$^{-/-}$ cells treated with nocodazole formed kinetochore crescents containing Rod, CENP-E, and Mad1, but not CENP-F [12] (Figure 3A and Figure S3A). To ensure complete depletion and avoid postmitotic arrest [27], we deleted *BUB1* or its kinetochore scaffold *KNL1* [1, 2] in p53-deficient RPE cells. *KNL1*$^{-/-}$ cells formed crescents with normal levels of RZZ but slightly less Mad1 (22% reduction; Figure 3B and Figure S3B). However deleting *BUB1* or *KNL1* decreased the period of nocodazole-induced mitotic arrest by 76% and 93% (median $T_{mitosis}$=130 min for *KNL1*$^{-/-}$ cells and 460 min for *BUB1*$^{-/-}$ cells, versus 1935 min for control cells), indicating that that SAC signaling was functionally compromised.

Although kinetochores in *BUB1*$^{-/-}$ and *KNL1*$^{-/-}$ cells have high levels of Mad1-Mad2, we could not exclude the possibility that a small but functionally important pool was missing. Therefore we tested the consequences of deleting *BUB1* or *KNTC1* and simultaneously expressing a constitutively kinetochore-bound form of Mad1 (Mis12-Mad1) that is refractory to SAC silencing at metaphase [28] (Figure 3D-J). Mis12-Mad1 expression triggered a mitotic arrest in *KNTC1*$^{-/-}$ cells that was even longer (median $T_{mitosis}$=1170 min) than that observed in wildtype cells expressing Mis12-Mad1 (median $T_{mitosis}$=780 min; Figure 3I). This hyperactive response likely reflects RZZ's role in stripping Mad1 and other SAC mediators from metaphase kinetochores via dynein-dependent transport [29–31]. In contrast *BUB1*$^{-/-}$ cells had a much weaker response to Mis12-Mad1 kinetochore tethering (median $T_{mitosis}$=130 min; Figure 3J). We next combined Mis12-Mad1 expression with nocodazole treatment to eliminate dynein-dependent stripping and engage upstream SAC signaling. This regimen further extended the mitotic arrest in *KNTC1*$^{-/-}$ cells (median $T_{mitosis}$=1355 min, versus 1560 min for wildtype cells) but accelerated mitotic exit in *BUB1*$^{-/-}$ cells (median $T_{mitosis}$=240 min) relative to nocodazole treatment alone (median $T_{mitosis}$=460 min; Figure 3I-J). We conclude that Mad1-Mad2 tethering can bypass RZZ, but not Bub1, with respect to SAC signaling. Our findings suggest that RZZ's crucial and likely sole function in SAC activation is to maintain Mad1-Mad2 at kinetochores, whereas RZZ-dependent corona formation is not required. In contrast Bub1 is not required for RZZ to localize at kinetochores, form the fibrous corona, or recruit Mad1-Mad2. However Mad1-Mad2 still requires a non-receptor activity of Bub1 to generate a "wait anaphase" signal.

## *BUB1*-disrupted clones re-express Bub1 and regain SAC function via nonsense-associated alternative splicing

The SAC defect we observed after acute *BUB1* disruption is consistent with studies in *Bub1* conditional-knockout MEFs [9, 32] but not with recent studies in *BUB1*-disrupted human cell clones [33–35] (Figure 4A). To understand the basis of this discrepancy, we isolated 13

clones after acute disruption of *BUB1* in p53-deficient RPE cells. All clones exhibited a partial (3–30%) recovery of Bub1 expression, kinetochore localization, and H2A kinase activity as judged by IFM with antibodies that recognize Bub1's N-terminus and T120-phosphorylated H2A (Figure 4B-E). We performed RT-PCR and sequencing on five clones (Figure 4F and Data S1). Full-length *BUB1* transcripts harbored exon 4 indels that induce frameshift and early termination (Figure S4A). We also observed shorter transcripts that skipped part or all of exon 4 and/or utilized cryptic splice sites (Figure S4B-F). A number of alternatively spliced transcripts encoded *BUB1* ORFs with short N-terminal deletions or insertions, thus explaining Bub1 re-expression (Figure S4C-F). Eleven of 13 clones exhibited partial or complete recovery of SAC function relative to acute deletion of *BUB1* (Figure 4G). Among the five clones analyzed by RT-PCR and sequencing, clone 12 was fully SAC-proficient and had the highest rate of in-frame transcripts (6 of 36), whereas clone 21 had intermediate SAC function and a lesser rate (3 of 31). No in-frame transcripts were identified in clone 8 (0 of 18) and clone 24 (0 of 21), which were the most SAC-defective (Figure 4G). Taken together, these results suggest that nonsense-associated alternative splicing (NAS) [36] attenuates and in some cases suppresses the effects of null mutations in *BUB1*. Our findings demonstrate how genome editing can trigger both acute loss of function and compensatory changes in mRNA structure that result in phenocopying of unedited cells.

## Discussion

In cells treated with spindle poisons, Mad1-Mad2 remains bound to kinetochores and catalyzes MCC production for 1000 min or more, thus extending mitosis at least 30-fold. How (and why) this sustained response occurs is not well understood. In yeast, Bub1 is the sole receptor for Mad1-Mad2 and required for the SAC [37], but models for Mad1-Mad2 regulation in mammalian cells differ considerably [7–12]. In our studies, acute *BUB1* or *KNL1* deletion led to SAC failure despite high levels of Mad1-Mad2 at kinetochores. Furthermore $BUB1^{-/-}$ cells were largely unresponsive to Mis12-Mad1, which is constitutively tethered to kinetochores and cannot be silenced at metaphase. Similar results were obtained independently using a Ndc80-Mad1 fusion [35]. These data strongly suggest a non-receptor function of Bub1-KNL1 that is required for kinetochore-bound Mad1-Mad2 to inhibit anaphase. One possibility is that Bub1 functions as a co-catalyst in MCC assembly by recruiting Cdc20 to kinetochores [7, 38]. Asking if this occurs *in vivo* will require SAC-independent methods for synchronizing $BUB1^{-/-}$ and $KNL1^{-/-}$ cells in mitosis in sufficient quantity and purity for biochemical studies of MCC assembly [39] or tools SAC-dependent synchronization.

Our studies also shed light on RZZ's role in the SAC. By tracking Mad1 dynamics with high temporal resolution, we demonstrate that kinetochores in early mitotic cells can recruit Mad1-Mad2 without RZZ and can delay anaphase onset by 100–300 min, thus mitigating the impact of less efficient chromosome congression in RZZ-null cells. However kinetochores with attachment defects that persist beyond this timeframe require RZZ to recruit Mad1-Mad2 and maintain SAC arrest. Expressing Mis12-Mad1 reinstated long-term arrest in $KNTC1^{-/-}$ cells, suggesting that RZZ's crucial and perhaps only role in the SAC is to tether Mad1-Mad2 to kinetochores. It has been proposed that RZZ mediates SAC signaling at unattached but not tensionless kinetochores [10]. However $KNTC1^{-/-}$ cells

challenged with spindle poisons that block attachment (nocodazole) or permit attachment without tension (STLC and taxol) escaped SAC arrest with similar kinetics (Figure 1B).

RZZ is also implicated in formation of the fibrous corona, a structural expansion of the outer kinetochore that precedes microtubule attachment [4, 6, 17]. Kinetochore expansion depends on mitotic kinases [5, 13], but relevant phosphorylation events are not known. We identified two Mps1-regulated phosphosites just upstream of Rod's β-propeller domain [24] that are required for kinetochore expansion but not SAC arrest. Rod and Spindly not only interact via this domain [14, 20] but also inhibit their own assembly into polymers [13, 40]. Together, these findings suggest that phosphorylation alleviates a structural barrier to Spindly-RZZ polymerization.

In this study and others [3, 27, 39, 41, 42], we used genome editing to delete or disrupt exons of genes involved in cell division. Normally this results in a "knockout" because of nonsense-mediated decay (NMD), a pathway that degrades mRNAs with premature termination codons (PTCs) [43, 44]. However PTCs can also trigger NAS, a less well-understood pathway in which splicing rules are relaxed to bypass the PTC and restore expression of near-full length ORFs [36, 45, 46]. NAS could also explain why *BUB1* exon 2-disrupted HeLa cells manifest a clear SAC defect after *BUB1* exon 8-specific RNAi [35]. In conclusion, NMD and NAS have opposite effects on the expressivity and penetrance of nonsense mutations, and should not be overlooked in the design, analysis, and interpretation of genome editing experiments.

## STAR Methods

### CONTACT FOR REAGENT AND RESOURCE SHARING

Further information and requests for resources and reagents should be directed to and will be fulfilled by the Lead Contact, Prasad Jallepalli (jallepap@mskcc.org).

### EXPERIMENTAL MODEL AND SUBJECT DETAILS

**Cell lines and chemicals—**Cell lines used in this study are described in the Key Resource Table. HeLa (human cervical adenocarcinoma, female) and HEK293 (human embryonic kidney, female) derivatives were grown at 37°C in Dulbecco's modifi ed eagle medium (DMEM) with 10% tetracycline free fetal bovine serum, 100 U/ml penicillin, and 100 U/ml streptomycin. hTERT-RPE (human retinal pigment epithelium, female) derivatives were grown at 37°C in a 1:1 mixture of DMEM and Ham's F- 12 medium with 10% fetal bovine serum, 100 U/ml penicillin, and 100 U/ml streptomycin, and 2.5 mM L-glutamine. HCT116 (human colorectal adenocarcinoma, male) were grown at 37°C in McCoy's 5A medium with 10% fetal bovine serum, 100 U/ml penicillin, and 100 U/ml streptomycin. Unless stated otherwise, nocodazole (660 nM), taxol (1 μM), S-trityl-L-cysteine (10 μM), MG132 (10 μM), hesperadin (100 nM), ZM447439 (2 μM), reversine (500 nM), and FTI-288 (10 μM) were used at the indicated concentrations.

## METHOD DETAILS

**Transgene expression—**LAP-Rod (WT or 2A) was cloned into pcDNA5/FRT/TO. Constructs were cotransfected with pOG44 into HeLa T-Rex Flp-In cells using FuGene 6 (Roche). Integrants were selected using hygromycin (0.2 mg/ml), picked as single colonies, and induced with doxycycline (0.8 μg/ml). mCherry-Mis12-Mad1 [28] was cloned into a piggyBac vector containing a doxycycline-inducible promoter (*tetON*) and constitutively expressing reverse tetracycline transactivator (*rtTA*) and neomycin phosphotransferase (*neoR*) linked by the self-cleaving T2A peptide. HeLa cells were cotransfected with this construct and pSuperPiggyBac transposase (System Biosciences), selected in G418 (0.5 mg/ml), and induced as above. For stable expression of FLAP-Mad1, EGFP-CENP-A, and H2B-mCherry, retroviral transfer plasmids were cotransfected with pVSV-G into Phoenix 293 cells. For stable expression of mRuby-CENP-A or gene-specific sgRNAs, lentiviral transfer plasmids were cotransfected with psPAX2 and pMD2.G into Lenti-X 293T cells (Clontech). 24 to 48 hr later, supernatants were filtered, mixed 1:1 with fresh medium containing polybrene (20 μg/ml), and applied to target cells for 24 hr. Transductants were selected in G418, blasticidin (5 μg/ml), or puromycin (5 to 20 μg/ml).

**AAV-mediated gene targeting—**5’ and 3’ homology arms encompassing *KNTC1* exons 2 and 3 were amplified from human BAC clone RP11–18E11 using Pfusion DNA polymerase. A new *loxP* site was added upstream of exon 2 via XbaI digest and linker ligation. The entire targeting construct was transferred to pAAV as a NotI fragment. All manipulated regions were checked by sequencing to ensure their integrity. Procedures for preparing infectious AAV particles, transducing HCT116 cells, and isolating correctly targeted clones were performed as described [48]. The *FRT-neo*$^{R}$*-FRT* cassette was excised through transient expression of FLP recombinase (pCAGGS-FLPe) and limiting dilution. To delete *KNTC1*$^{HF}$, cells were infected with AdCre (Vector Development Laboratory, Baylor College of Medicine).

**CRISPR/Cas9-mediated genome editing—**Zifit (http://zifit.partners.org/ZiFiT/ChoiceMenu.aspx) and sgRNA Designer (http://www.broadinstitute.org/rnai/public/analysis-tools/sgrna-design) were used to identify and rank candidate CRISPR/Cas9 targets for predicted on- and off-target activities. For transient expression, sequences were ordered as overlapping 60-nt oligonucleotides, annealed and extended into a 100-bp duplex using Pfusion DNA polymerase, and cloned into an AflII-digested guide RNA expression vector (Addgene 41824) by Gibson assembly. Equal amounts of human codon-optimized Cas9 (Addgene 41815) and sgRNA vectors were transfected into HCT116 cells using FuGene 6 and into RPE cells using a Nucleofector 2b device (Lonza). For stable expression, target sequences were ordered as 24-nt oligonucleotides with asymmetric 5’ overhangs, phosphorylated with T4 polynucleotide kinase, then annealed and cloned into BsmBI-digested lentiGuide-puro (Addgene 52963) or pLenti-sgRNA (Addgene 71409) using T4 DNA ligase. Lentiviral transduction was performed as described above. Gene deletion was initiated by inducing a doxycycline-regulated Cas9 transgene present in the host cell line [27] or by infection with AdCas9 (ViraQuest).

**Immunofluorescence microscopy and live-cell imaging—**Antibodies used in this study are listed in the Key Resource Table. Cells were fixed and permeabilized in PEMFT (20 mM PIPES, pH 6.8, 10 mM EGTA, 1 mM $MgCl_2$, 4% paraformaldehyde, and 0.2% Triton X-100) for 13 min, blocked in 4% BSA, and stained with primary antibodies overnight. Species-specific secondary antibodies conjugated to Alexa Fluor 488, 564, or 647 were applied for 1 hr. Coverslips were mounted in ProLong Gold, imaged with a 100x oil objective on a DeltaVision Elite microscope (GE Life Sciences), and deconvolved in SoftWoRx using measured point spread functions. For timelapse experiments cells were grown in multiwell plates or 35 mm glass-bottom dishes (MatTek) and imaged on a Nikon Eclipse Ti microscope equipped with a stage-top incubator and $CO_2$ delivery system, 20x and 40x air objectives and 60x (1.4 NA) and 100x (1.45 NA) oil objectives, a Yokogawa CSU-X1 unit, and sCMOS (Andor Xyla 5.5) and EMCCD (Photometrics Evolve 512) cameras. Acquisition was performed with NIS Elements (v5.41). Epifluorescence and/or DIC images were acquired at 10-min intervals to measure mitotic arrest in response to spindle poisons, or at 2-min intervals to measure unperturbed mitotic timing. Confocal imaging of FLAP-Mad1 and H2B-mCherry was performed at 2- to 5-min intervals. Fluorescence intensities were quantified in ImageJ (v1.51) and analyzed in Prism 7.0 (GraphPad).

**Correlative light-electron microscopy—**Cells were fixed with 2.5% glutaraldehyde (Sigma) in PBS, pH 7.4–7.6 for 30 min, rinsed with PBS (3 × 5 min), and mounted in Rose chambers. Multimode (DIC and 3-color fluorescence) datasets were obtained on a Nikon TE2000 microscope equipped with a PlanApo 100× 1.45 NA objective lens at 53-nm XY pixels and 200-nm Z-steps. All LM images were deconvolved in SoftWoRx (v5.0) with lens-specific PSFs. Post-fixation, embedding, and sectioning were done as previously described [47]. Thin sections (70–80 nm) were imaged on a JEOL 1400 microscope operated at 80 kV using a side-mounted 4.0 megapixel XR401 sCMOS AMT camera (Advanced Microscopy Techniques Corp). Full series of images recorded at 10K magnification were used to reconstruct the volume of the cell, match orientation and superimpose this volume on the corresponding LM dataset. Higher-magnification images (40K) were then collected for individual kinetochores.

**Cell lysis, immunoprecipitation, and Western blotting—**Cell extracts were prepared by resuspending pellets in ice-cold buffer B (140 mM NaCl, 30 mM HEPES, pH 7.8, 5% glycerol, 10 mM sodium pyrophosphate, 5 mM sodium azide, 10 mM NaF, 10 mM PMSF, 0.3 mM sodium orthovanadate, 20 mM b-glycerophosphate, 1 mM DTT, 0.2 mM microcystin, and 1x protease inhibitor cocktail (Sigma)) prior to nitrogen cavitation (1250 psi, 45 min; Parr Instruments) and centrifugation at 20,000 x g for 30 min. LAP-Rod was immunoprecipitated with GFP antibodies coupled to protein G-Dynabeads using bis(sulfosuccinimidyl)suberate (BS3). Zw10 was immunoprecipitated without BS3 crosslinking. Extracts and immunoprecipitates were separated by SDS-PAGE and transferred to PVDF or nitrocellulose membranes. Membranes were blocked and probed with primary antibodies and secondary antibody-HRP conjugates in 5% nonfat dry milk in TBST (Tris-buffered saline + 0.05% Tween-20) before detecting signals via enhanced chemiluminescence (Western Lightning Plus, PerkinElmer).

**RT-PCR and sequencing—**Total RNA was purified (RNeasy Mini kit, Qiagen) and reverse-transcribed with random hexamers (SuperScript IV First-Strand Synthesis System, ThermoFisher). RT reactions were diluted 100-fold and amplified with *BUB1*-specific primers spanning exons 2–6 or exons 3–8. PCR products were cloned into pCR4 (TOPO-TA Cloning Kit, ThermoFisher) and sequenced with M13 reverse primer. Reads were trimmed and aligned in SeqMan Pro and annotated in SeqBuilder (DNASTAR LaserGene v14).

### QUANTIFICATION AND STATISTICAL ANALYSIS

Quantitative data was compiled in Excel and analyzed using Prism 7.0. Details of each statistical analysis (number of cells (n), number of experiments (N), and measures of central tendency (mean or median)) are specified in the figure legends and Results. Unless stated otherwise, error bars indicate SEM. $P \leq 0.05$ (with adjustment for multiple-hypothesis testing where applicable) was used as the significance threshold.

## Supplementary Material

Refer to Web version on PubMed Central for supplementary material.

## Acknowledgments

We thank George Church, Didier Trono, David Sabatini, and Feng Zhang for sharing plasmids through Addgene. P.V.J. was supported by NIH grants R01GM094972 and P30CA008748.

## References

1. London N, and Biggins S (2014). Signalling dynamics in the spindle checkpoint response. Nat Rev Mol Cell Biol 15, 736–747. [PubMed: 25303117]
2. Musacchio A (2015). The Molecular Biology of Spindle Assembly Checkpoint Signaling Dynamics. Curr Biol 25, R1002–1018. [PubMed: 26485365]
3. Rodriguez-Bravo V, Maciejowski J, Corona J, Buch HK, Collin P, Kanemaki MT, Shah JV, and Jallepalli PV (2014). Nuclear pores protect genome integrity by assembling a premitotic and mad1-dependent anaphase inhibitor. Cell 156, 1017–1031. [PubMed: 24581499]
4. Magidson V, Paul R, Yang N, Ault JG, O'Connell CB, Tikhonenko I, McEwen BF, Mogilner A, and Khodjakov A (2015). Adaptive changes in the kinetochore architecture facilitate proper spindle assembly. Nat Cell Biol 17, 1134–1144. [PubMed: 26258631]
5. Wynne DJ, and Funabiki H (2015). Kinetochore function is controlled by a phospho-dependent coexpansion of inner and outer components. J Cell Biol 210, 899–916. [PubMed: 26347137]
6. Hoffman DB, Pearson CG, Yen TJ, Howell BJ, and Salmon ED (2001). Microtubule-dependent changes in assembly of microtubule motor proteins and mitotic spindle checkpoint proteins at PtK1 kinetochores. Molecular biology of the cell 12, 1995–2009. [PubMed: 11451998]
7. Vleugel M, Hoek TA, Tromer E, Sliedrecht T, Groenewold V, Omerzu M, and Kops GJ (2015). Dissecting the roles of human BUB1 in the spindle assembly checkpoint. J Cell Sci 128, 2975–2982. [PubMed: 26148513]
8. Klebig C, Korinth D, and Meraldi P (2009). Bub1 regulates chromosome segregation in a kinetochore-independent manner. J Cell Biol 185, 841–858. [PubMed: 19487456]
9. Zhang G, Lischetti T, Hayward DG, and Nilsson J (2015). Distinct domains in Bub1 localize RZZ and BubR1 to kinetochores to regulate the checkpoint. Nature communications 6, 7162.
10. Silio V, McAinsh AD, and Millar JB (2015). KNL1-Bubs and RZZ Provide Two Separable Pathways for Checkpoint Activation at Human Kinetochores. Dev Cell 35, 600–613. [PubMed: 26651294]

11. Caldas GV, Lynch TR, Anderson R, Afreen S, Varma D, and DeLuca JG (2015). The RZZ complex requires the N-terminus of KNL1 to mediate optimal Mad1 kinetochore localization in human cells. Open biology 5.
12. Raaijmakers JA, van Heesbeen R, Blomen VA, Janssen LME, van Diemen F, Brummelkamp TR, and Medema RH (2018). BUB1 Is Essential for the Viability of Human Cells in which the Spindle Assembly Checkpoint Is Compromised. Cell reports 22, 1424–1438. [PubMed: 29425499]
13. Sacristan C, Ahmad MUD, Keller J, Fermie J, Groenewold V, Tromer E, Fish A, Melero R, Carazo JM, Klumperman J, et al. (2018). Dynamic kinetochore size regulation promotes microtubule capture and chromosome biorientation in mitosis. Nat Cell Biol 20, 800–810. [PubMed: 29915359]
14. Gama JB, Pereira C, Simoes PA, Celestino R, Reis RM, Barbosa DJ, Pires HR, Carvalho C, Amorim J, Carvalho AX, et al. (2017). Molecular mechanism of dynein recruitment to kinetochores by the Rod-Zw10-Zwilch complex and Spindly. J Cell Biol 216, 943–960. [PubMed: 28320824]
15. Saurin AT, van der Waal MS, Medema RH, Lens SM, and Kops GJ (2011). Aurora B potentiates Mps1 activation to ensure rapid checkpoint establishment at the onset of mitosis. Nature communications 2, 316.
16. Santaguida S, Vernieri C, Villa F, Ciliberto A, and Musacchio A (2011). Evidence that Aurora B is implicated in spindle checkpoint signalling independently of error correction. EMBO J 30, 1508–1519. [PubMed: 21407176]
17. McEwen BF, Arena JT, Frank J, and Rieder CL (1993). Structure of the colcemid-treated PtK1 kinetochore outer plate as determined by high voltage electron microscopic tomography. J Cell Biol 120, 301–312. [PubMed: 8421050]
18. Schmitt HD (2010). Dsl1p/Zw10: common mechanisms behind tethering vesicles and microtubules. Trends Cell Biol 20, 257–268. [PubMed: 20226673]
19. Civril F, Wehenkel A, Giorgi FM, Santaguida S, Di Fonzo A, Grigorean G, Ciccarelli FD, and Musacchio A (2010). Structural analysis of the RZZ complex reveals common ancestry with multisubunit vesicle tethering machinery. Structure 18, 616–626. [PubMed: 20462495]
20. Mosalaganti S, Keller J, Altenfeld A, Winzker M, Rombaut P, Saur M, Petrovic A, Wehenkel A, Wohlgemuth S, Muller F, et al. (2017). Structure of the RZZ complex and molecular basis of its interaction with Spindly. J Cell Biol
21. Basto R, Scaerou F, Mische S, Wojcik E, Lefebvre C, Gomes R, Hays T, and Karess R (2004). In vivo dynamics of the rough deal checkpoint protein during Drosophila mitosis. Curr Biol 14, 56–61. [PubMed: 14711415]
22. Cooke CA, Schaar B, Yen TJ, and Earnshaw WC (1997). Localization of CENP-E in the fibrous corona and outer plate of mammalian kinetochores from prometaphase through anaphase. Chromosoma 106, 446–455. [PubMed: 9391217]
23. Rattner JB, Rao A, Fritzler MJ, Valencia DW, and Yen TJ (1993). CENP-F is a .ca 400 kDa kinetochore protein that exhibits a cell-cycle dependent localization. Cell Motil Cytoskeleton 26, 214–226. [PubMed: 7904902]
24. Maciejowski J, Drechsler H, Grundner-Culemann K, Ballister ER, Rodriguez-Rodriguez JA, Rodriguez-Bravo V, Jones MJK, Foley E, Lampson MA, Daub H, et al. (2017). Mps1 Regulates Kinetochore-Microtubule Attachment Stability via the Ska Complex to Ensure Error-Free Chromosome Segregation. Dev Cell 41, 143–156 e146. [PubMed: 28441529]
25. Holland AJ, Reis RM, Niessen S, Pereira C, Andres DA, Spielmann HP, Cleveland DW, Desai A, and Gassmann R (2015). Preventing farnesylation of the dynein adaptor Spindly contributes to the mitotic defects caused by farnesyltransferase inhibitors. Molecular biology of the cell 26, 1845–1856. [PubMed: 25808490]
26. Moudgil DK, Westcott N, Famulski JK, Patel K, Macdonald D, Hang H, and Chan GK (2015). A novel role of farnesylation in targeting a mitotic checkpoint protein, human Spindly, to kinetochores. J Cell Biol 208, 881–896. [PubMed: 25825516]
27. McKinley KL, and Cheeseman IM (2017). Large-Scale Analysis of CRISPR/Cas9 Cell-Cycle Knockouts Reveals the Diversity of p53-Dependent Responses to Cell-Cycle Defects. Dev Cell 40, 405–420 e402. [PubMed: 28216383]

28. Maldonado M, and Kapoor TM (2011). Constitutive Mad1 targeting to kinetochores uncouples checkpoint signalling from chromosome biorientation. Nat Cell Biol 13, 475–482. [PubMed: 21394085]
29. Gassmann R, Holland AJ, Varma D, Wan X, Civril F, Cleveland DW, Oegema K, Salmon ED, and Desai A (2010). Removal of Spindly from microtubule-attached kinetochores controls spindle checkpoint silencing in human cells. Genes Dev 24, 957–971. [PubMed: 20439434]
30. Howell BJ, McEwen BF, Canman JC, Hoffman DB, Farrar EM, Rieder CL, and Salmon ED (2001). Cytoplasmic dynein/dynactin drives kinetochore protein transport to the spindle poles and has a role in mitotic spindle checkpoint inactivation. J Cell Biol 155, 1159–1172. [PubMed: 11756470]
31. Silva PM, Reis RM, Bolanos-Garcia VM, Florindo C, Tavares AA, and Bousbaa H (2014). Dynein-dependent transport of spindle assembly checkpoint proteins off kinetochores toward spindle poles. FEBS letters 588, 3265–3273. [PubMed: 25064841]
32. Perera D, Tilston V, Hopwood JA, Barchi M, Boot-Handford RP, and Taylor SS (2007). Bub1 maintains centromeric cohesion by activation of the spindle checkpoint. Dev Cell 13, 566–579. [PubMed: 17925231]
33. Currie CE, Mora-Santos MD, Smith C, McAinsh AD, and Millar JB (2018). Bub1 is not required for the checkpoint response to unattached kinetochores in diploid human cells. bioRxiv
34. Raaijmakers JA, Tanenbaum ME, Maia AF, and Medema RH (2009). RAMA1 is a novel kinetochore protein involved in kinetochore-microtubule attachment. J Cell Sci 122, 2436–2445. [PubMed: 19549680]
35. Zhang G, Kruse T, and Nilsson J (2018). The RZZ complex facilitates Mad1 binding to Bub1 ensuring efficient checkpoint signaling. bioRxiv
36. Cartegni L, Chew SL, and Krainer AR (2002). Listening to silence and understanding nonsense: exonic mutations that affect splicing. Nature reviews. Genetics 3, 285–298.
37. London N, and Biggins S (2014). Mad1 kinetochore recruitment by Mps1-mediated phosphorylation of Bub1 signals the spindle checkpoint. Genes Dev 28, 140–152. [PubMed: 24402315]
38. Faesen AC, Thanasoula M, Maffini S, Breit C, Muller F, van Gerwen S, Bange T, and Musacchio A (2017). Basis of catalytic assembly of the mitotic checkpoint complex. Nature 542, 498–502. [PubMed: 28102834]
39. Maciejowski J, George KA, Terret ME, Zhang C, Shokat KM, and Jallepalli PV (2010). Mps1 directs the assembly of Cdc20 inhibitory complexes during interphase and mitosis to control M phase timing and spindle checkpoint signaling. J Cell Biol 190, 89–100. [PubMed: 20624902]
40. Gassmann R, Pereira C, Reis RM, Gama JB, Cheerambathur DK, and Carvalho AX (2018). Self-assembly of the RZZ complex into filaments drives kinetochore expansion in the absence of microtubule attachment. bioRxiv
41. Tsou M-FB, Wang W-J, George KA, Uryu K, Stearns T, and Jallepalli PV (2009). Polo kinase and separase regulate the mitotic licensing of centriole duplication in human cells. Developmental Cell 17, 344–354. [PubMed: 19758559]
42. McKinley KL, Sekulic N, Guo LY, Tsinman T, Black BE, and Cheeseman IM (2015). The CENP-L-N Complex Forms a Critical Node in an Integrated Meshwork of Interactions at the Centromere-Kinetochore Interface. Mol Cell 60, 886–898. [PubMed: 26698661]
43. Popp MW, and Maquat LE (2016). Leveraging Rules of Nonsense-Mediated mRNA Decay for Genome Engineering and Personalized Medicine. Cell 165, 1319–1322. [PubMed: 27259145]
44. Lykke-Andersen S, and Jensen TH (2015). Nonsense-mediated mRNA decay: an intricate machinery that shapes transcriptomes. Nature Reviews Molecular Cell Biology 16, 665. [PubMed: 26397022]
45. Anderson JL, Mulligan TS, Shen MC, Wang H, Scahill CM, Tan FJ, Du SJ, Busch-Nentwich EM, and Farber SA (2017). mRNA processing in mutant zebrafish lines generated by chemical and CRISPR-mediated mutagenesis produces unexpected transcripts that escape nonsense-mediated decay. PLoS Genet 13, e1007105. [PubMed: 29161261]

46. Mou H, Smith JL, Peng L, Yin H, Moore J, Zhang XO, Song CQ, Sheel A, Wu Q, Ozata DM, et al. (2017). CRISPR/Cas9-mediated genome editing induces exon skipping by alternative splicing or exon deletion. Genome biology 18, 108. [PubMed: 28615073]

47. Magidson V, He J, Ault JG, O'Connell CB, Yang N, Tikhonenko I, McEwen BF, Sui H, and Khodjakov A (2016). Unattached kinetochores rather than intrakinetochore tension arrest mitosis in taxol-treated cells. J Cell Biol 212, 307–319. [PubMed: 26833787]

48. Berdougo E, Terret M, and Jallepalli P (2009). Functional dissection of mitotic regulators through gene targeting in human somatic cells. Methods Mol Biol 545, 21–37. [PubMed: 19475380]

## Highlights

- RZZ mediates a temporal switch in how Mad1-Mad2 is recruited to kinetochores
- Mps1 phosphorylates Rod's N-terminus to trigger fibrous corona formation
- Mad1-Mad2 requires a non-receptor activity of Bub1 to inhibit anaphase
- Nonsense-associated alternative splicing can circumvent *BUB1* disruption

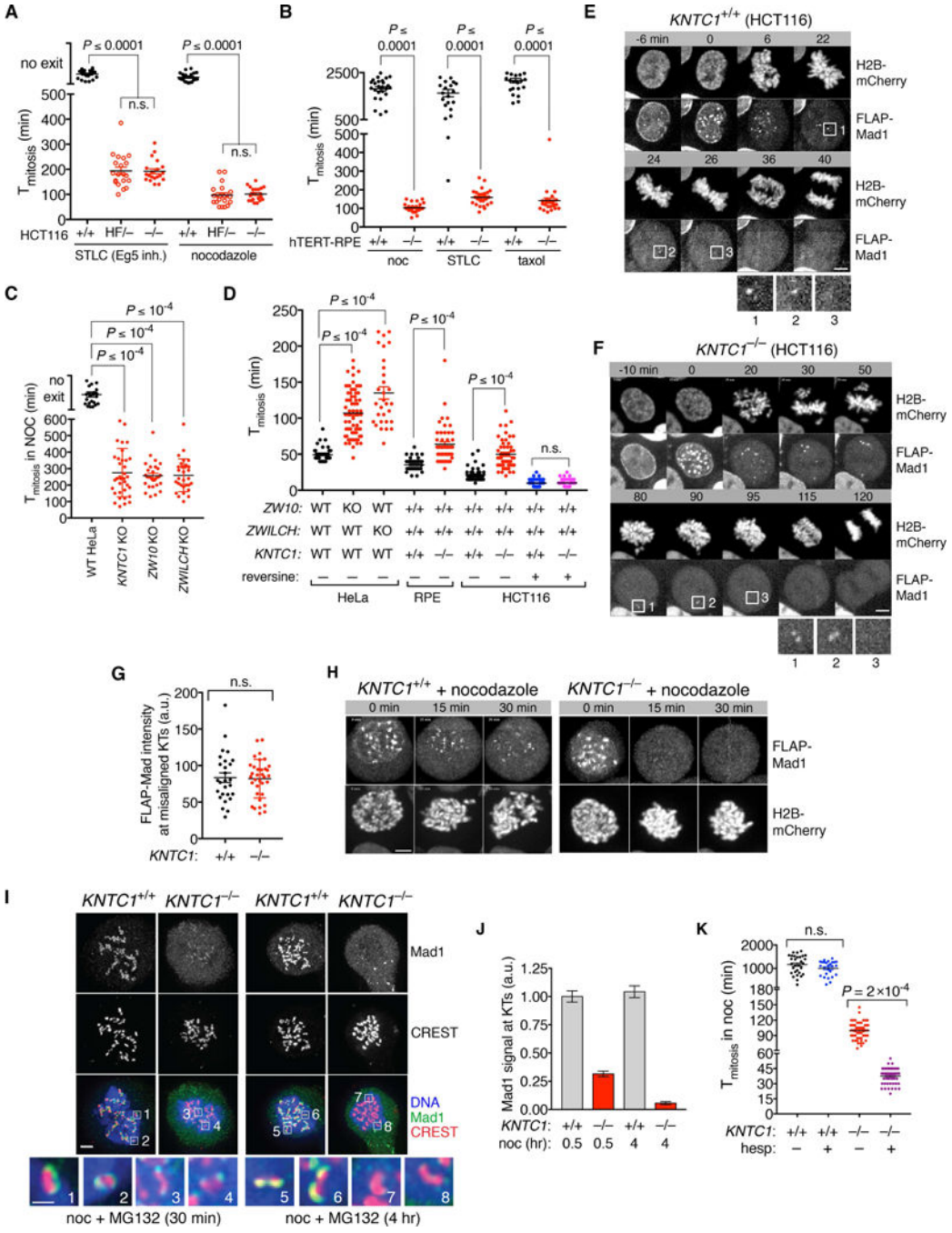


**Figure 1. A temporal switch in the requirements for Mad1-Mad2 targeting to kinetochores during SAC signaling.**

(A) AAV- and CRISPR-mediated genome editing was used to modify the *KNTC1* locus in HCT116 cells (Figure S1A-E). Cells expressing H2B-mCherry were treated with nocodazole or STLC and followed by epifluorescence and DIC timelapse microscopy. Images were acquired at 10-min intervals. Mitotic duration (from NEBD to chromatin decondensation) was quantified in at least 25 cells per condition per experiment (N=2). *P*-values were computed using Kruskal-Wallis and Dunn's multiple comparisons tests. Error bars throughout the paper indicate s.e.m. unless stated otherwise. (B) Wildtype and *KNTC1*$^{-/-}$

RPE1 cells (Figure S1F-I) were treated with nocodazole, STLC, or taxol and followed using DIC optics. Cell rounding (mitotic entry) and cortical blebbing and flattening (mitotic exit) were used as landmarks. (C) Clonal HeLa *KNTC1*, *ZW10*, and *ZWILCH* knockouts [27] were treated with nocodazole and followed as in (B). (D) Mitotic timing in unperturbed wildtype and RZZ-deficient HeLa, RPE, and HCT116 cells. Where indicated Mps1 kinase was inhibited with reversine. (E and F) Wildtype and *KNTC1*$^{-/-}$ HCT116 cells expressing H2B-mCherry and FLAP-Mad1 were filmed during unperturbed mitosis using spinning disk confocal microscopy. Insets show enlarged views of FLAP-Mad1 recruitment to and dissociation from kinetochores. Scale bars throughout the paper are 10 μm unless stated otherwise. See also Videos S1 and S2. (G) Quantification of FLAP-Mad1 at misaligned chromosomes in (E) and (F). (H) Cells in (E) and (F) were filmed in the presence of nocodazole (n=6 for wildtype and n=14 for *KNTC1*$^{-/-}$). (I and J) Wildtype and *KNTC1*-null RPE cells were treated with nocodazole and MG132 for 30 min or 4 hours before fixation for IFM. Mad1/CREST fluorescence intensity ratios were determined for at least 100 kinetochores in 5 cells per condition (N=3). (K) Wildtype and *KNTC1*-null RPE cells were treated with nocodazole in the presence or absence of hesperadin (hesp) to inhibit Aurora B kinase. Mitotic duration was determined from 30 cells per condition. See also Figure S1.

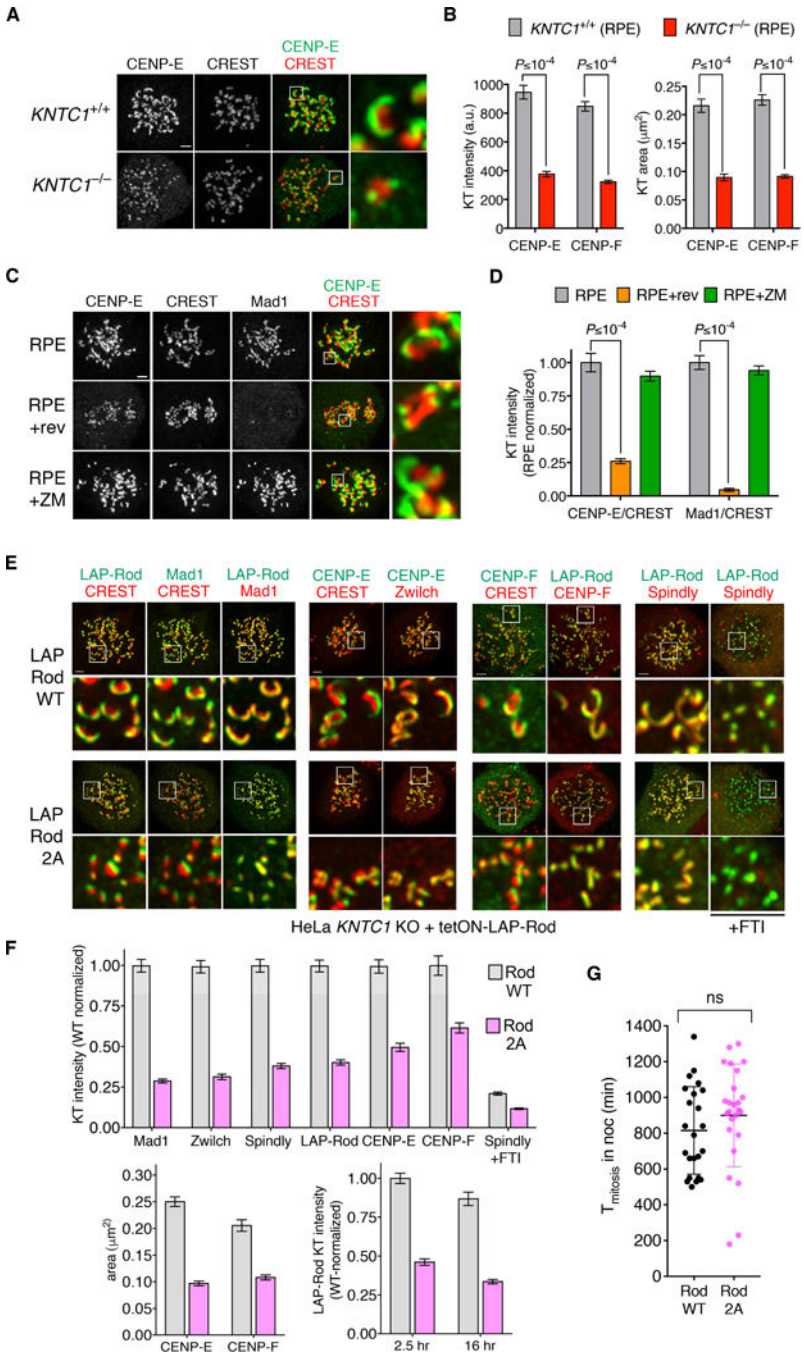


**Figure 2. Mps1 phosphorylation at the N-terminus of Rod triggers RZZ-dependent kinetochore expansion.**

(A and B) Wildtype and *KNTC1*$^{-/-}$ RPE cells were treated with nocodazole and MG132 for 2.5 hours before IFM with antibodies to CENP-E (A) or CENP-F (Figure S2A). Crescent size and intensity were determined in 5 to 10 cells (N=3). (C and D) RPE cells were treated with nocodazole and MG132 for 2 hr, after which reversine (rev) or Aurora B inhibitor ZM447439 (ZM) was added or omitted for 1 hr (n=10 cells, N=3). CREST-normalized kinetochore intensities of Mad1 and CENP-E were determined by IFM. (E and F) *KNTC1*-null HeLa cells reconstituted with LAP-Rod$^{WT}$ or LAP-Rod$^{2A}$ were treated with nocodazole

for 2.5 hr. IFM was used to visualize crescents and quantify kinetochore-associated LAP-Rod, Mad1, CENP-E, CENP-F, Spindly, and CREST (n=100 kinetochores in 5 cells each, N=2). Where indicated, cells were treated with the farnesyltransferase inhibitor FTI-288 (FTI) as a positive control for blockade of Spindly targeting to kinetochores [25, 26]. Note that kinetochores in LAP-Rod$^{2A}$ cells remained compact during long-term SAC arrest (16 hr nocodazole treatment). (G) The duration of mitotic arrest in nocodazole-treated LAP-Rod$^{WT}$ and LAP-Rod$^{2A}$ cells was determined by DIC timelapse (n≥50 cells, N=2) and compared using the Mann-Whitney U test. See also Figure S2.

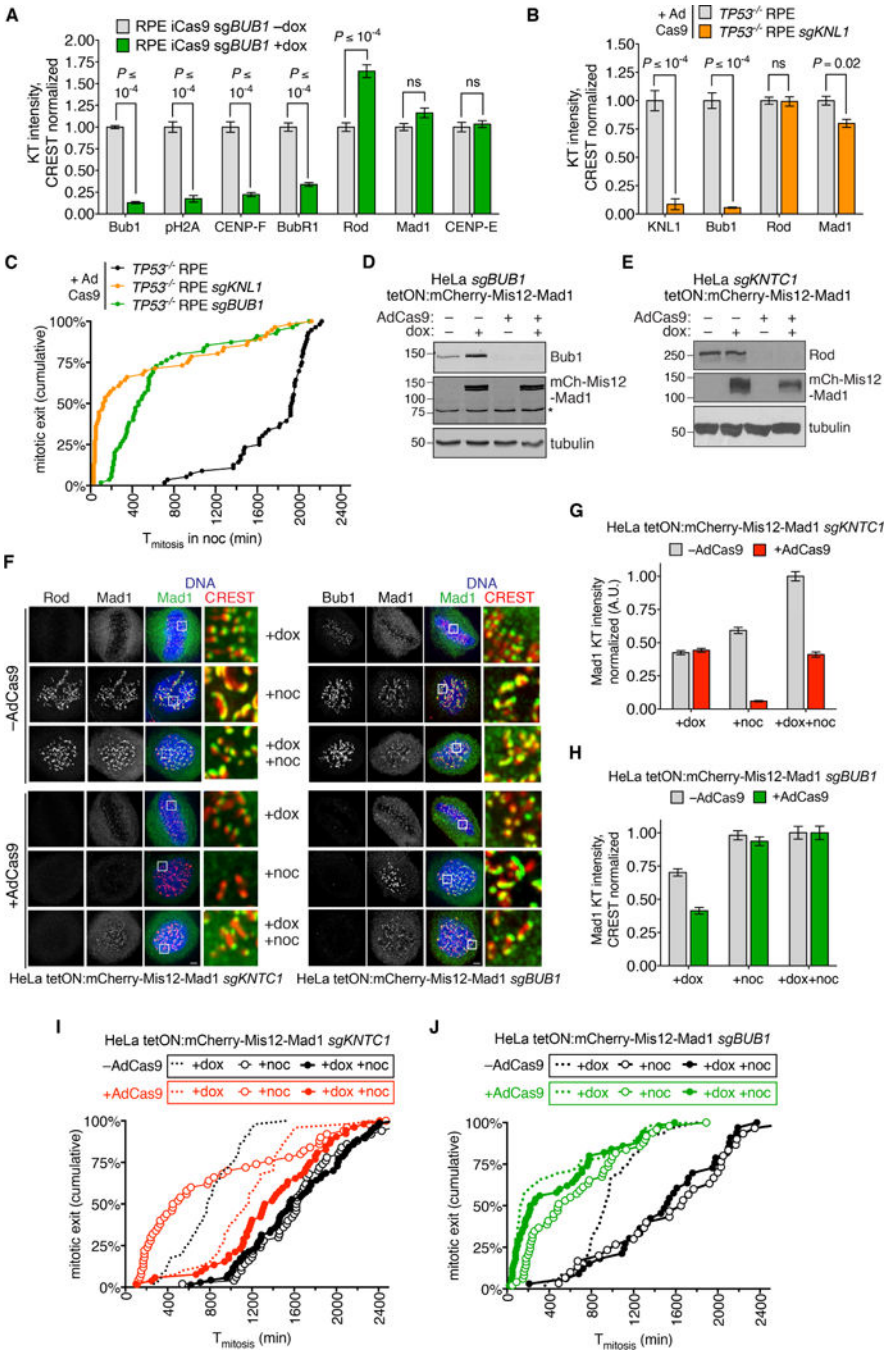


**Figure 3. RZZ and Bub1-KNL1 have distinct roles in recruiting and activating Mad1-Mad2 at kinetochores during SAC signaling.**

(A) RPE iCas9 cells expressing *sgBUB1* were treated with or without doxycycline and analyzed by IFM after 5 days (for images see Figure S3A). (B) *TP53*$^{-/-}$ RPE cells with or without *sgKNL1* were treated with AdCas9 and analyzed by IFM after three days (for images see Figure S3B). (C) AdCas9-treated cells were filmed in the presence of nocodazole for 48 hours. Cumulative frequency of mitotic exit is plotted. (D and E) HeLa cells expressing *BUB1*- or *KNTC1*-specific sgRNA were treated with AdCas9. After three days, mCherry-Mis12-Mad1 was induced with doxycycline for 17 hr. Protein depletion or

expression was confirmed by Western blotting. (F-H) Cells in (D and E) were analyzed by IFM, either with or without a further 3-hr treatment with nocodazole. Mad1/CREST ratios were determined for ≥100 kinetochores in 5 cells (N=2). (I and J) Cells in (D and E) were treated with doxycycline and/or nocodazole and followed by DIC timelapse (n≥50 cells, N=2). See also Figure S3.

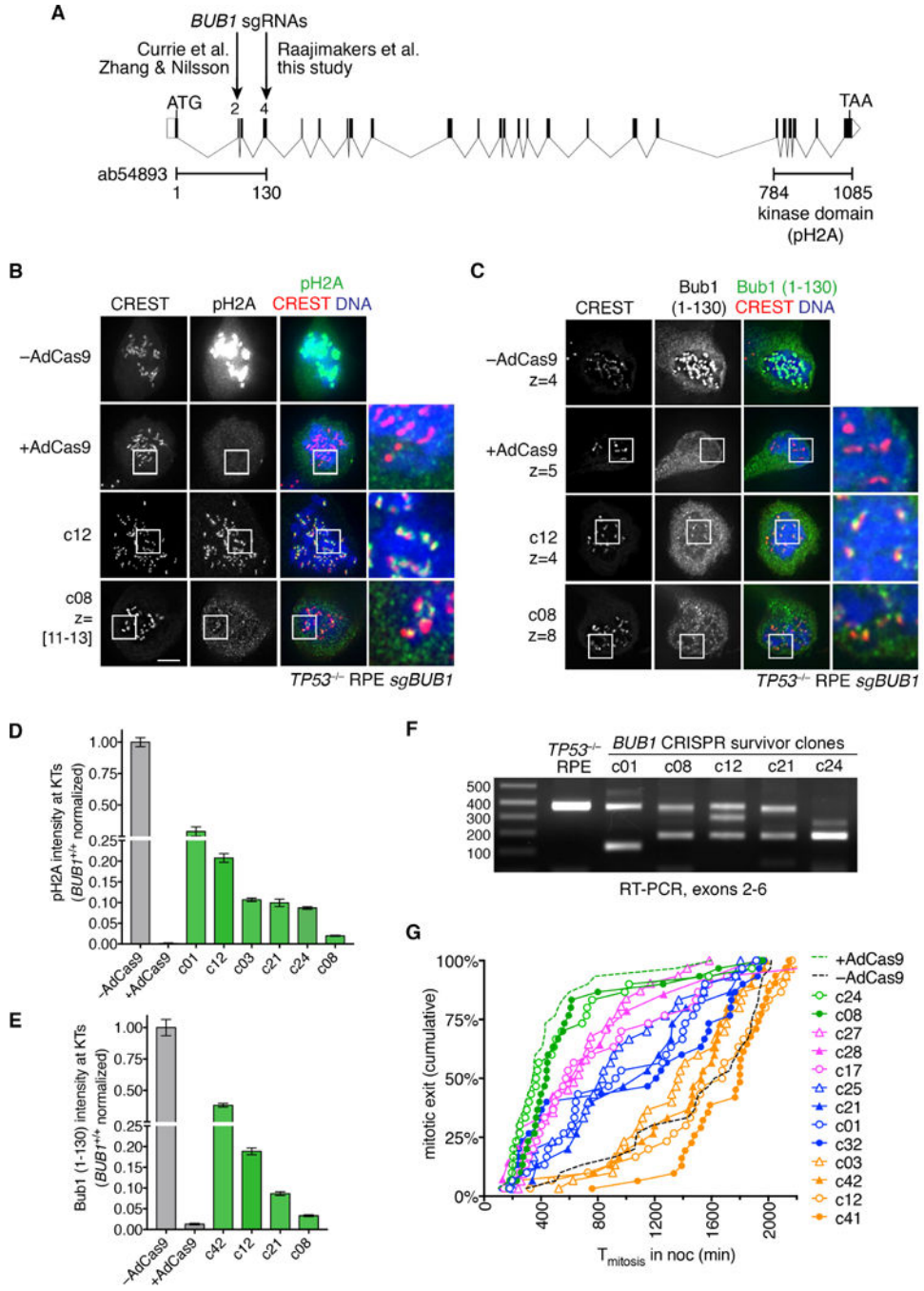


**Figure 4. *BUB1*-disrupted clones regain Bub1 expression and SAC function through nonsense-associated alternative splicing.**

(A) Structure of the *BUB1* locus. Locations of guide RNAs used in this and previous studies [33–35] are shown. Regions encoding N-terminal Bub1 antibody epitope and C-terminal kinase domain are indicated. (B-E). Parental *TP53*$^{-/-}$ RPE cells (–AdCas9), acute *BUB1* knockout cells (+AdCas9), and *BUB1*-disrupted clones (c12, c08) were treated with nocodazole and MG132 for 2 hr. Centromeric H2A phosphorylation (B and D) and kinetochore-associated Bub1 (C and E) were quantified by IFM (n=100 kinetochores in 5 cells, N=2). Where indicated, individual z-slices or maximum intensity projections of

adjacent z-slices are displayed. For all other images, maximum intensity projections of full z-series are shown. (F) RNA samples were reverse-transcribed and amplified with PCR primers spanning exons 2–6. (G) *BUB1*-disrupted clones were treated with nocodazole and followed by DIC timelapse. Parental *TP53*$^{-/-}$ RPE cells (–AdCas9) and acute *BUB1* knockout cells (+AdCas9) were used as controls. See also Figure S4 and Data S1.

## KEY RESOURCES TABLE

| REAGENT or RESOURCE | SOURCE | IDENTIFIER |
|---|---|---|
| Antibodies | | |
| CREST (human) | Immunovision | HCT-0100; RRID: AB_2744669 |
| Rod (mouse) | Santa Cruz | sc-81853; RRID: AB_2133542 |
| Zw10 (rabbit) | Abcam | ab21582; RRID: AB_779030 |
| Zwilch (mouse) | A. Musacchio | N/A |
| Mad1 (mouse) | A. Musacchio | clone BB3–8 |
| Mad2 (rabbit) | Bethyl | A300–301A; RRID: AB_2281536 |
| Bub1 (rabbit) | Genetex | GTX107497; RRID: AB_1949770 |
| Bub1 (mouse) | Abcam | ab54893; RRID: AB_940664 |
| BubR1 (mouse) | BD Biosciences | BD612503; RRID: AB_2066085 |
| KNL1 (rabbit) | Bethyl | A300–804A; RRID: AB_577218 |
| Spindly (rabbit) | Bethyl | A301–354A; RRID: AB_937753 |
| CENP-E (mouse) | Abcam | ab5093; RRID: AB_304747 |
| CENP-F (rabbit) | Novus | NB500–101; RRID: AB_2229328 |
| p150$^{glued}$ (mouse) | BD Biosciences | BD612708; RRID: AB_399947 |
| phospho-T210 H2A (rabbit) | Active Motif | 39391; RRID: AB_2744670 |
| phospho-T13/S15 Rod (rabbit) | Jallepalli Lab [24] | N/A |
| EGFP (mouse) | Santa Cruz | sc-9996; RRID: AB_627695 |
| EGFP (mouse) | ThermoFisher | A-11120 (clone 3E6); RRID: AB_221568 |
| EGFP (rabbit) | Jallepalli Lab [24] | N/A |
| α-tubulin (mouse) | Santa Cruz | sc-5286; RRID: AB_628411 |
| α-tubulin (rat) | Chemicon | MAB1864 (clone YL½); RRID: AB_2210391 |
| mCherry (rabbit) | ThermoFisher | PA5–34974; RRID: AB_2552323 |
| mCherry (mouse) | Abcam | ab125096; RRID: AB_11133266 |
| Bacterial and Virus Strains | | |
| AdCas9 | ViraQuest | N/A |
| Ad5 CMV Cre | Vector Development Lab, Baylor College of Medicine | Lot#032415 |
| | | |
| Biological Samples | | |
| | | |
| | | |
| | | |
| | | |
| | | |
| Chemicals, Peptides, and Recombinant Proteins | | |
| Nocodazole | Sigma | Cat#M1404; CAS:31430–18-9 |
| Taxol (Paclitaxel) | Sigma | Cat#T7402; CAS:254753–54-3 |

| REAGENT or RESOURCE | SOURCE | IDENTIFIER |
|---|---|---|
| S-Trityl-L-cysteine (STLC) | ThermoFisher | Cat#2191; CAS:2799–07-7 |
| MG132 | Selleckchem | Cat#S2619; CAS:133407–82-6 |
| Hesperidin | Selleckchem | Cat#S2309; CAS:520–26-3 |
| ZM447439 | Tocris | Cat#2458; CAS:331771–20-1 |
| Reversine | Cayman Chemical | Cat#10004412; CAS:656820–32-5 |
| FTI-277 | Sigma | Cat#F9803; CAS:170006–73-2 |
| G418 | Corning | Cat#61234-RF; CAS:108321–42-2 |
| Blasticidin | ThermoFisher | Cat#A1113903; CAS:2079–00-7 |
| Puromycine | ThermoFisher | Cat#A1113803; CAS: 58–58-2 |
| Hygromycin | Calbiochem | Cat#400051; CAS: 31282–04-9 |
| FuGene 6 | Promega | Cat#E2691 |
| SuperScript IV First-Strand Synthesis System | ThermoFisher | Cat#18091050 |
| TOPO-TA Cloning Kit | ThermoFisher | Cat#450071 |
| | | |
| Critical Commercial Assays | | |
| | | |
| | | |
| | | |
| | | |
| | | |
| Deposited Data | | |
| | | |
| | | |
| | | |
| | | |
| | | |
| Experimental Models: Cell Lines | | |
| HEK293 | ATCC | CCL-1573 |
| Lenti-X 293T | Clontech | 632180 |
| Phoenix-GP293 | ATCC | CCL-3215 |
| HCT116 | ATCC | CCL-247 |
| HCT116 KNTC1 (HF/+) | this study | N/A |
| HCT116 KNTC1 (HF/-) | this study | N/A |
| HCT116 KNTC1 (−/−) | this study | N/A |
| HeLa | ATCC | CCL-2 |
| HeLa + sgKNTC1 | this study | N/A |
| HeLa TetON-mCherry-Mis12-Mad1 | this study | N/A |
| HeLa TetON-mCherry-Mis12-Mad1 + sgKNTC1 | this study | N/A |
| HeLa TetON-mCherry-Mis12-Mad1 + sgBub1 | this study | N/A |

| REAGENT or RESOURCE | SOURCE | IDENTIFIER |
|---|---|---|
| HeLa iCas9 | Cheeseman Lab [27] | N/A |
| HeLa iCas9 KNTC1 KO | Cheeseman Lab [27] | Subcloned after sgKNTC1 + dox |
| HeLa iCas9 ZW10 KO | Cheeseman Lab [27] | Subcloned after sgZW10 + dox |
| HeLa iCas9 ZWILCH KO | Cheeseman Lab [27] | Subcloned after sgZWILCH + dox |
| HeLa Flp-In T-Rex | S. Taylor | N/A |
| HeLa Flp-In T-Rex LAP-Rod WT (KNTC1 KO) | this study | Subcloned after sgKNTC1 + AdCas9 |
| HeLa Flp-In T-Rex LAP-Rod 2A (KNTC1 KO) | this study | Subcloned after sgKNTC1 + AdCas9 |
| RPE1 | Clontech | now ATCC CRL-4000 |
| RPE1 KNTC1(−/−) | this study | Subcloned after cotransfection with KNTC1 gRNA vectors (tru1 + tru5) and Cas9 |
| RPE1 iCas9 | Cheeseman Lab [27] | N/A |
| RPE1 iCas9 + sgBUB1 | Cheeseman Lab [27] | N/A |
| RPE1 TP53(−/−) | this study | Subcloned after cotransfection with TP53 gRNA vector and Cas9 |
| RPE1 TP53(−/−) + sgBUB1 | this study | N/A |
| RPE1 TP53(−/−) + sgKNL1 | this study | N/A |
| | | |
| Experimental Models: Organisms/Strains | | |
| | | |
| | | |
| | | |
| | | |
| | | |
| | | |
| Oligonucleotides | | |
| | | |
| | | |
| | | |
| | | |
| | | |
| Recombinant DNA | | |
| pcDNA5/FRT/TO | ThermoFisher | V6520–20 |
| pcDNA5/FRT/TO-LAP-Rod (WT) | this study | N/A |
| pcDNA5/FRT/TO-LAP-Rod (2A) | this study | N/A |
| pOG44 | ThermoFisher | V6005–20 |
| PB-tetON-mCherry-Mis12-Mad1 | this study | N/A |
| pSuperPiggyBac transposase | System Biosciences | PB210PA-1 |
| pAAV-lacZ | Agilent | AAV Helper-Free System (240071) |
| pRC | Agilent | AAV Helper-Free System (240071) |
| pHelper | Agilent | AAV Helper-Free System (240071) |

| REAGENT or RESOURCE | SOURCE | IDENTIFIER |
|---|---|---|
| pAAV-KNTC1-HF | this study | N/A |
| pCAGGS-FLPe | GeneBridges | A201 |
| pVSV-G | Clontech | PT3343–5 |
| pQCXIN-FLAP-Mad1 | Jallepalli Lab [3] | N/A |
| pQCXIB-H2B-mCherry | Jallepalli Lab [3] | N/A |
| pQCXIB-GFP-CENP-A | this study | N/A |
| empty gRNA vector | G. Church | Addgene 41824 |
| TP53 gRNA vector; target GGCAGCTACGGTTTCCGTC | M.-F. Tsou | N/A |
| KNTC1.tru1 gRNA vector; target GTGGCCACTAAACACTTC | this study | N/A |
| KNTC1.tru5 gRNA vector; target GTGGACGTTATTCCTAA | this study | N/A |
| human codon-optimized Cas9 | G. Church | Addgene 41815 |
| psPAX2 | D. Trono | Addgene 12260 |
| pMD2.G | D. Trono | Addgene 12259 |
| lenti-sgRNA | D. Sabatini | Addgene 71409 |
| lentiguide-puro | F. Zhang | Addgene 52963 |
| lentiguide-puro-sgKNL1; target TAATTTAAAGCTTGAGAGCG | this study | N/A |
| lenti-sgKNTC1; target CCCGCCCAGGCAATGTACAG | Cheeseman Lab [27] | N/A |
| lenti-sgBUB1; target CTTTTCTTGAACCGACACTC | Cheeseman Lab [27] | N/A |
| lenti-sgZWILCH; target CTTTGCTGATCAACTGCAGT | Cheeseman Lab [27] | N/A |
| lenti-sgZW10; target CAAAACTTCTGTCACGAACC | Cheeseman Lab [27] | N/A |
| Software and Algorithms | | |
| Zifit | Zinc Finger Consortium | http://zifit.partners.org |
| sgRNA Designer | Broad Institute | http://www.broadinstitute.org |
| SoftWoRx | GE Healthcare | https://www.gelifesciences.com |
| NIS Elements v5.41 | Nikon | https://www.nikoninstruments.com RRID:SCR_014329 |
| ImageJ v1.51 | NIH | https://imagej.nih.gov RRID:SCR_003070 |
| Prism 7.0 | GraphPad | https://www.graphpad.com RRID:SCR_002798 |
| Lasergene v14 | DNASTAR | https://www.dnastar.com |
| Other | | |
| | | |
| | | |
| | | |
| | | |
| | | |